Analysis of the Carrier-Induced FM Response of DFB Lasers: Theoretical and Experimental Case Studies

PATRICK VANKWIKELBERGE, FILIP BUYTAERT, ANN FRANCHOIS, ROEL BAETS, MEMBER, IEEE, P. I. KUINDERSMA, AND C. W. FREDRIKSZ

Abstract—**A comprehensive analysis of the carrier-induced FM response of DFB lasers is given both in theory and by experiment.**

Experimentally it is found that the FM response may sometimes vary (strongly) from chip to chip. In a number of cases anomalies either as a function of frequency or as a function of bias are observed.

Theoretically, a new dynamic model is presented which includes spectral as well as longitudinal spatial hole burning. The main feature of the model is that local variations of the Bragg wavelength caused by hole burning, are rigorously and self-consistently taken into account.

By comparing the experimental results with theoretical calculations, it is shown that spatial hole burning is an important phenomenon in DFB lasers. The model confirms that the dynamic (FM) behavior can strongly vary from DFB chip to DFB chip. The model shows that spatial hole burning is indeed the dominant factor which induces the anomalies that are found experimentally in the FM response.

I. Introduction

THE dynamic single-mode DFB laser is one of the most promising and practical candidates as a light source for optical coherent communication systems. In particular, optical FSK heterodyne detection systems are attractive. They pose only moderate requirements on the laser linewidth, and the frequency modulation is obtained by directly modulating the DFB laser. The FM response of the latter then is a quantity of prime interest.

Recently, some research groups have reported theoretical and experimental results on the dynamics of DFB lasers [1]–[7]. Their work covers the IM and FM response of DFB lasers with and without phase-tuning segments. The models used for explaining the experimental results are usually derived from the simple rate equations [8] for Fabry–Perot lasers.

In this paper we give a detailed analysis of the FM modulation behavior of DFB lasers in the frequency range where thermal effects no longer affect the small-signal behavior, i.e., above about 50 MHz. First we will give examples of experimental data on the FM response of DFB lasers. Then a model is presented in which spatial (longitudinal), temporal, and spectral effects are taken into account simultaneously. Next this model is applied to a number of DFB lasers and also to a Fabry–Perot laser. Finally, a discussion is given in which the experimental and theoretical results are compared.

Manuscript received December 12, 1988; revised June 9, 1989. This work was supported in part by the European RACE Project R1010 (CMC). The work of P. Vankwikelberge was supported by the Belgian National Fund for Scientific Research (NFWO).

P. Vankwikelberge, F. Buytaert, A. Franchois, and R. Baets are with the Laboratory of Electromagnetism and Acoustics, University of Ghent—IMEC, B-9000 Ghent, Belgium.

P. I. Kuindersma and C. W. Fredriksz are with Philips Research Laboratories, 5600 JA Eindhoven, The Netherlands.

IEEE Log Number 8930601.

II. Experimental Investigation

A. The DFB Devices

The FM response as a function of frequency and of bias was measured for as-cleaved as well as for asymmetrically-coated DFB lasers with a first-order grating ($\lambda = 1.55\ \mu m$). The investigated frequency range usually ran from 100 MHz to 4 GHz, at output powers up to approximately 10 mW. Prior to measuring their FM response the devices were selected for genuine single-mode behavior; i.e., they show an SMSR (side mode suppression ratio) of more than 30 dB over a wide power and temperature range (10–60°C). The asymmetrically-coated DFB's had either a 5 or a 0.4 percent front-facet reflectivity, and an as-cleaved back facet. The transverse structure of the devices is of the PB-DCPBH-type [9], where the proton bombardment (PB) is used to enhance the bandwidth of the devices (with IM 3 dB bandwidths up to 6 GHz). Typical thresholds are around 20 mA, for devices of 250 μm length. Inferred from stopband measurements below threshold, the optical-wave-grating coupling κL is about 2.

B. FM Response Measurements

The FM response at a given frequency and bias was measured by adding a small ac component to the dc bias, while measuring the power spectrum of the optical output by a scanning Fabry–Perot interferometer. The amplitude ΔI of the ac current was adjusted such as to obtain a power spectrum of the frequency-modulated lightwave with a known FM index. Particular useful FM indexes in this respect are, e.g., $m = 2.4$ (zero amplitude for the carrier frequency), $m = 1.4$ (with equal intensity for carrier and first sidebands), and $m = 1$ (with first sideband intensities

0018-9197/89/1100-2239$01.00

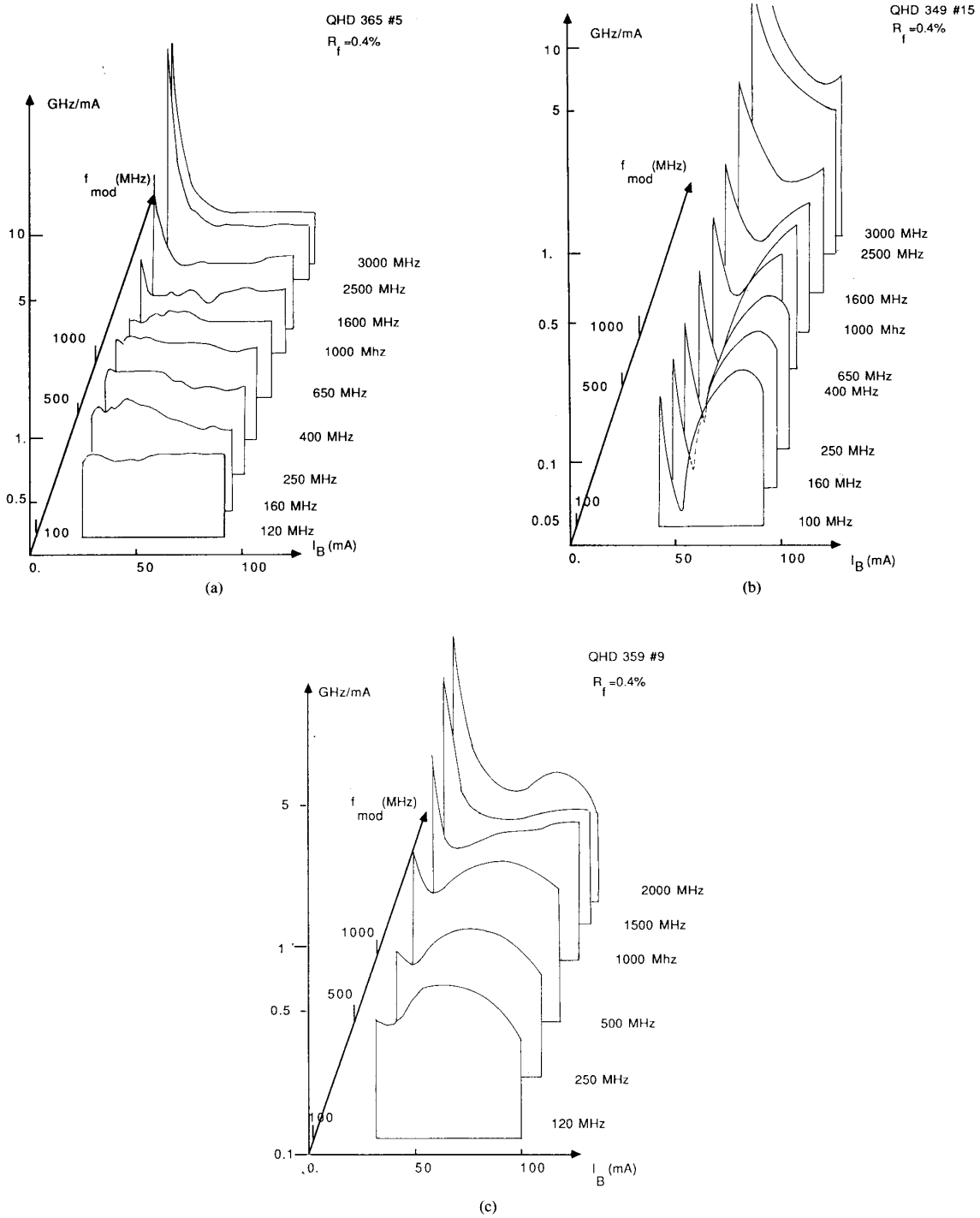

Fig. 1. (a)-(c) Perspective view of the FM response versus bias and frequency, for three SM-DFB lasers with a front-facet reflectivity R_f = 0.4 percent.

equal to one-third of the carrier). Using the relation between FM index m and frequency sweep $\Delta f\,(= mf_{\mathrm{mod}})$ the FM response follows from $df/dI = (mf_{\mathrm{mod}})/\Delta I$.

Particularly at high modulation frequency f_{mod} the data were checked for consistency, at various values for the FM index, in order to exclude the residual amplitude or other spurious modulation that would spoil the experimental data. Moreover, great care was taken to avoid the effect of (weak) reflections back into the laser cavity on the FM response of the DFB lasers.

C. Examples of Measured FM Responses

Compared to the regular behavior of the (small-signal) intensity modulation response of (FP and) DFB lasers, the measured behavior of the corresponding FM response as a function of frequency and bias is complex.

The small-signal intensity modulation (IM) response basically is frequency independent up to a few GHz, followed by the relaxation oscillation contribution at higher frequencies. Below the relaxation oscillation at f_r the IM response is also bias independent, whereas f_r is roughly equal to 1 GHz/$\sqrt{\text{mA}}$ bias above threshold. For DFB lasers there is some scatter from chip to chip in the level of the IM response: the random facet phases cause some scatter in the front-facet differential efficiency. In contrast, the corresponding FM responses, however, turned out to be chip dependent, bias dependent, and frequency dependent. By chip dependent we do not mean a dependence on the particular chip type (be it uncoated, or asymmetrically coated with either 5 or 0.4 percent facet reflectivity), but just a (sometimes large) variation from chip to chip, apparently independent of the chip type. By bias and frequency dependent we specifically refer to peculiar dependencies, at frequencies below the relaxation oscillation frequency (in the range from 100 MHz to a few GHz).

Below we give an account of the FM response of some 15 measured DFB devices, while trying to find in the description a balance between general features and many exceptions. The number of devices is too small to carry out good statistics. We therefore restrict ourselves to giving examples.

Fig. 1(a)–(c) give a general, perspective overview of the FM response of three chips as a function of bias and modulation frequency. All three devices have the same front-facet reflectivity (0.4 percent), but behave quite differently. The device of Fig. 1(a) shows the most simple behavior: an FM response, fairly independent of both frequency and bias, except at low bias/high frequency, where the relaxation oscillation enhances the FM response.

The most pronounced feature in the FM response of the device of Fig. 1(b) is the occurrence of a steep dip at a bias of approximately 50 mA. This pronounced dip as function of bias is not due to or associated with a mode jump or the rise of a second mode.

The perspective view of the FM response of the device of Fig. 1(c) looks intermediate between that of the chips of (a) and (b): a little pronounced dip as a function of bias is observed, and the FM response shows some frequency dependence.

Instead of the instructive perspective views of Fig. 1(a)–(c), the FM response can also be drawn in a more practical form as a function of frequency at various bias levels. Fig. 2(a) gives such a plot for the device of Fig. 1(a), showing that the FM is not really frequency independent at higher bias. Fig. 2(b) gives the corresponding plot for the device of Fig. 1(b), showing that in the pronounced dip at 50 mA bias, the FM response (above 300 MHz) is proportional to the modulation frequency. At still higher bias we find a well-behaved, almost flat response at frequencies up to about 1 GHz.

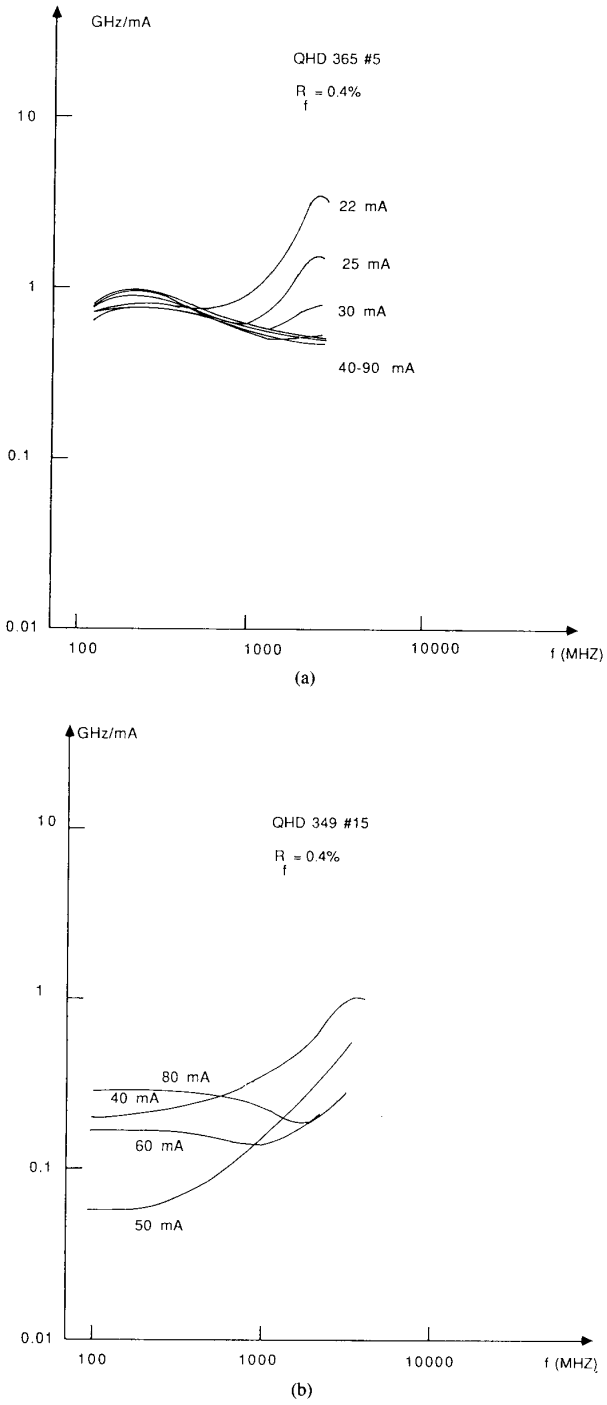

Fig. 2. The FM response as a function of frequency at various bias levels. The device of (a) is the same as that of Fig. 1(a), whereas (b) corresponds to Fig. 1(b). Both devices have an R_f of 0.4 percent.

The example of Fig. 3 shows a device with 2 uncoated facets. The device also shows an FM response proportional to the frequency (below the relaxation oscillation), also at one specific bias level, but now at about 3 mA above threshold. This illustrates that the dip as a function of bias not only occurs for (some) devices with specifi-

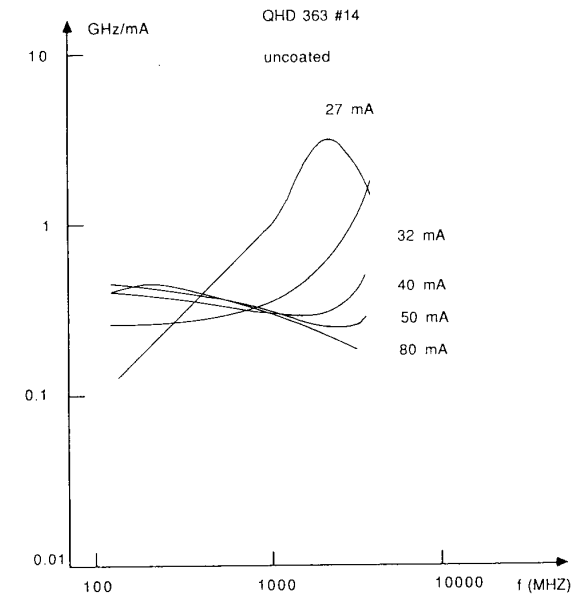

Fig. 3. The FM response of a 1.55 μm SM-DFB device with uncoated facets, as a function of frequency at various bias levels.

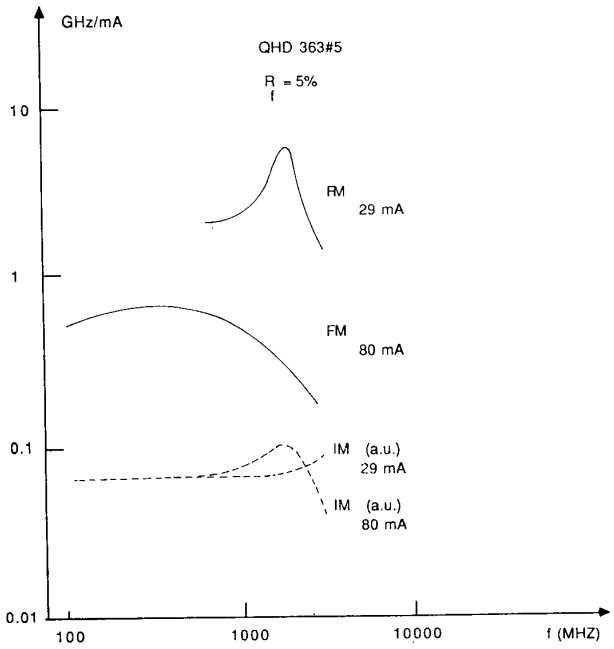

Fig. 4. Comparison between (relative) IM response (in a.u.l.) and FM response as a function of frequency, at low and high bias. The 1.55 μm SM-DFB has an R_f of 5 percent.

cally a 0.4 percent front-facet reflectivity. At high bias levels, the FM response resembles the response of the device of Fig. 1(a) [or Fig. 2(a)], with a decrease above approximately 1 GHz.

The reader may get the impression that a dip in the FM response as a function of bias is the rule. However, this is not the case. The FM response for a device with a 5

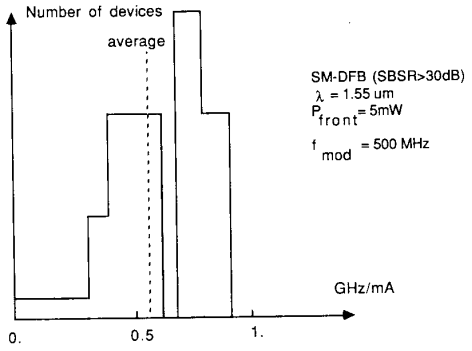

Fig. 5. Distribution of the FM efficiency of SM-DFB's at 5 mW front-facet power output and a modulation frequency of 500 MHz.

percent front-facet reflectivity, at low and at high bias, is given in Fig. 4. The figure again illustrates that the various responses are not specific for a particular front-mirror reflectivity. This device does not exhibit the dip as function of bias, but shows only a moderate and gradual decrease of the FM level with increasing bias. In the figure, for comparison the corresponding (relative) IM responses are also shown. At a few mA bias above threshold the FM and IM show the relaxation oscillation; the FM level is rather high. At high bias the IM response is flat as a function of frequency, whereas the FM is only approximately flat from 100 MHz to 1 GHz and subsequently decreases roughly as $1/f$ when going beyond 1 GHz. The time scale of rolloff is also of interest: 3 dB rolloff around 1.5 GHz implies a characteristic time of about 0.10 ns, which is much shorter than the measured effective electronic lifetime at threshold (0.7 ns).

Given the different bias and frequency dependencies for the FM response of the various devices, there is some difficulty in comparing the level of the FM response for various devices. Fig. 5 gives such a distribution at a modulation frequency of 500 MHz and a front-facet output power of 5 mW.

III. A Simplified Physical Treatment of Carrier-Induced FM

Before proceeding towards an extensive theoretical analysis, a simple treatment of the carrier-induced FM response is given. This description focuses on the different physical phenomena involved.

The small-signal rate equation for the field intensity P can be written as

$$\frac{1}{v_g}\frac{dp}{dt} = \left(\frac{\partial G}{\partial P}p + \frac{\partial G}{\partial N}n - \frac{\partial L}{\partial P}p\right)P_o. \qquad (1)$$

Here p and n are the small-signal representations of the average optical field intensity $P(t) = P_o + p(t)$ and the average carrier density $N(t) = N_o + n(t)$, respectively. Furthermore, G is the net averaged gain per unit length, L represents the feedback loss, and v_g is the group velocity. This rate equation is an extended version of one that is found for example in [10]. The additional term $(\partial L/\partial P)\,p$ in (1) arises from a spatial modulation in the

carrier density along the laser cavity. It expresses the dependence of the feedback loss on the level of spatial hole burning, which in turn depends on the average power in the laser. In the frequency domain with modulation frequency $\Omega/2\pi$, (1) can also be written as

$$\frac{\partial G}{\partial N} n = \left(j\Omega \frac{1}{v_g} - \frac{\partial G}{\partial P} P_o + \frac{\partial L}{\partial P} P_o \right) \frac{p}{P_o}. \quad (2)$$

The small-signal equivalent for the field phase basically expresses that the round-trip phase in the cavity remains constant (modulo 2π). It can be cast in an expression which relates the frequency sweep $\Delta\omega$ to the real part of an effective refractive index modulation Δn_{re}

$$\frac{\Delta\omega}{v_g} + \frac{\omega}{c} \Delta n_{\text{re}} = 0. \quad (3)$$

In general, for distributed feedback, this effective index Δn_{re} differs from the average refractive index

$$\Delta \bar{n}_r = \int_o^L \Delta n_r(z)\, dz \quad (4)$$

where $\Delta n_r(z)$ is the local refractive index. Hence Δn_{re} is written as the sum

$$\Delta n_{\text{re}} = \Delta \bar{n}_r + \Delta n_L \quad (5)$$

in which Δn_L represents the direct influence of spatial hole burning on the spectral behavior of the phase of the distributed reflections. (One could compare this way of representation with replacing a change in cavity length by a fictitious change in refractive index.) This spatial hole burning dependence is again (as with L) represented by a power dependence of Δn_L (or Δn_{re}). The expression (3) then becomes

$$-\frac{\Delta\omega}{v_g} = \frac{\omega}{c} \frac{\partial n_{\text{re}}}{\partial N} n + \frac{\omega}{c} \frac{\partial n_{\text{re}}}{\partial P} p. \quad (6)$$

Now substituting the expression for the linewidth enhancement factor, i.e.,

$$\alpha = -2 \frac{\omega}{c} \left(\frac{\partial n_{\text{re}}}{\partial N} \Big/ \frac{\partial G}{\partial N} \right), \quad \text{with} \quad \frac{\partial n_{\text{re}}}{\partial N} = \frac{\partial \bar{n}_r}{\partial N} \quad (7)$$

and a similar expression for the relation between loss and index changes in the cavity, i.e.,

$$\beta = 2 \frac{\omega}{c} \left(\frac{\partial n_{\text{re}}}{\partial P} \Big/ \frac{\partial L}{\partial P} \right), \quad \text{with} \quad \frac{\partial n_{\text{re}}}{\partial P} = \frac{\partial n_L}{\partial P} \quad (8)$$

into (6) yields

$$\frac{1}{v_g} \Delta\omega = \frac{\alpha}{2} \frac{\partial G}{\partial N} n - \frac{\beta}{2} \frac{\partial L}{\partial P} p. \quad (9)$$

The second term to the right only arises when the feedback in the laser is distributed. Unlike the α, which is a conceptual "constant" [11], the factor β may differ from device to device, depending on details of the distributed feedback.

Substitution of (2) into (9) gives an expression which relates (small-signal) frequency sweep $\Delta\omega$ and intensity modulation p, i.e.,

$$\Delta\omega = \frac{\alpha}{2} \left[j\Omega \frac{1}{P_o} - \frac{\partial G}{\partial P} v_g + \left(1 - \frac{\beta}{\alpha} \right) \frac{\partial L}{\partial P} v_g \right] p. \quad (10)$$

As expressed by (10) there are in principle three, physically distinguishable, contributions to the FM response.

The Well-Known Ever-Present ("Relaxation Oscillation") Contribution, with $\Delta\omega = j\Omega(\alpha/2)(p/P_o)$: At frequencies below the relaxation oscillation frequency f_r, the IM response (p) is frequency and bias independent and hence, the FM response is proportional to the modulation frequency $\Omega/2\pi$ and to the inverse of the bias optical power level (P_o). In most situations anywhere near the relaxation oscillation, this term will not only be observed, but it will dominate.

The Contribution Due to Hole Burning in the Spectral Gain Profile, with $\Delta\omega = -(\alpha/2) v_g (\partial G/\partial P)\, p$: At frequencies below f_r this contribution to the FM response is frequency and bias independent. It should be stressed that spatial hole burning does not contribute to this term, as long as α is carrier concentration independent. The reason for this is simple, when one looks at the physics of spectral hole burning.

Spectral hole burning does not give rise to an increasing shortfall of carriers "at the laser frequency," but instead to an increasing excess of carriers at energies "outside the laser frequency." Obviously, the number of carriers "at the laser frequency" does not drop but remains constant, otherwise the device stops lasing. The increasing excess of carriers "outside the laser frequency" leads to a decreasing absorption $c \cdot q \cdot \Delta n_i$. Associated with this Δn_i at other wavelengths there is a decrease in the real part Δn_r at the lasing wavelength. The latter can be calculated via, e.g., a Kramers–Krönig relation.

Similar to spectral hole burning, spatial hole burning neither gives rise to an increasing shortfall of carriers "at the laser frequency," when averaged along the laser cavity. For spatial hole burning only, this implies however that (on the average) there is also no excess of carriers "outside the laser frequency" and hence no associated FM, unless the spatial hole burning affects the round-trip gain and phase conditions. If it does so, the third contribution arises.

The Contribution Due to the Influence of Spatial Hole Burning on the Cavity Losses and the Cavity Resonance Itself, with $\Delta\omega = (\alpha/2) v_g (1 - \beta/\alpha)(\partial L/\partial P)\, p$: With respect to this term it is instructive to consider first a Fabry–Perot laser cavity. Though appreciable spatial hole burning may occur there is no spatial contribution to the FM, simply because the feedback loss in such a cavity, $(1/L) \ln (1/R_f R_b)$, is independent of the power.

For DFB lasers the situation is very much different. There the feedback is caused by distributed Bragg reflections, which are determined by the precise values of facet reflectivities (modulus and especially phase), by the κL-

product [12] and by modulations on the uniformity of the grating (e.g., compare $\lambda/4$-shifted devices) [13]. Furthermore the spectral behavior of the distributed feedback is a sensitive function of internal carrier distribution and therefore of the power distribution in the laser [14]. Hence, when the power level changes with direct modulation, the amount of spatial hole burning changes. This in turn causes a shift in wavelength because the spatial hole burning affects the round-trip phase and the feedback losses, and consequently also the gain and carrier concentration. So basically, there are two contributions to this wavelength shift: a "direct" one related (via β) to the round-trip phase condition and an "indirect" one related (via α) to the unity round-trip gain condition. It should be realized that these two spatial hole burning contributions to the shift in wavelength however are interdependent.

At low frequencies the spatial hole burning FM contribution may be in-phase or out-of-phase with the spectral hole burning FM. At high frequencies (above the sum of 1/[carrier lifetime] and a characteristic spatial hole burning frequency) the spatial hole burning concentration will rolloff (in contrast to the fast spectral hole burning). In general the loss in DFB devices is affected by spatial hole burning in a nonlinear way. Therefore, one may expect the spatial hole burning FM to be bias dependent, in contrast with the bias independent spectral hole burning FM. A rough estimate of the rolloff frequency and of the bias dependence of the spatial hole burning is given in the Appendix.

Finally, we end this section with a remark on intensity modulation (IM). Spatial hole burning affects the loss in DFB laser cavities and hence the optical output. This implies in principle that the power differential efficiency also gets additional bias and frequency dependencies. However, relative to the implications for the FM response $\Delta\omega$, the effects on the IM response (p) are only minor, as can be seen for example from (10).

IV. A Rigorous Theoretical Treatment

The simple description given in the previous section focused on simplified physical phenomena (and is for DFB's strongly approximate). Here we give a thorough theoretical treatment, and present a new dynamic model which includes spectral as well as longitudinal spatial hole burning. The main feature of the model is that local variations of the Bragg wavelength caused by hole burning, are rigorously and self-consistently taken into account.

A. The Longitudinal Rate Equations

The dynamics of the optical field can be defined by a set of coupled traveling-wave rate equations. In the examples we will only consider lasers with a sufficient difference in loss between the lasing mode and the side modes. In this way we need to consider only the main lasing mode. The traveling wave rate equations are derived from Maxwell's equations using the slowly-varying amplitude approximation [15] and the approximations related to the coupled-mode theory [16]. The forward and backward propagating parts of the lateral electrical laser field of the considered TE-mode can be represented by

$$E_{y,F}(x, y, z, t) = \mathrm{Re}\left(R_F(z, t)e^{j(\omega t-\beta_g z)}\Phi(x, y)\right)$$
$$E_{y,B}(x, y, z, t) = \mathrm{Re}\left(R_B(z, t)e^{j(\omega t+\beta_g z)}\Phi(x, y)\right) \quad (11)$$

with $\beta_g = \pi/\Lambda$ for a first-order grating. $\Phi(x, y)$ is the transverse/lateral field distribution of the laser waveguide, assumed to be independent of time and axial position; ω is the lasing frequency. The complex amplitudes R_F and R_B satisfy the following equations and boundary conditions:

$$\frac{\partial R_F}{\partial z} + \frac{1}{v_g}\frac{\partial R_F}{\partial t} + j\Delta\beta(z, t)R_F = -j\kappa_{FB}R_B$$
$$-\frac{\partial R_B}{\partial z} + \frac{1}{v_g}\frac{\partial R_B}{\partial t} + j\Delta\beta(z, t)R_B = -j\kappa_{BF}R_F \quad (12)$$
$$R_F(0, t) = \rho_b R_B(0, t),$$
$$R_B(L, t) = \rho_f R_F(L, t)\exp\left(-2j\beta_g L\right) \quad (13)$$

with

$$\Delta\beta(z, t) = 2\pi n_e/\lambda - \beta_g + \Gamma\Delta\gamma - 0.5j\alpha_{\mathrm{int}}$$
$$\Delta\gamma = 2\pi/\lambda(\Delta n_r + j\Delta n_i) = \Delta\gamma_r + j\Delta\gamma_i$$
$$\Delta\gamma_r = -\alpha_{fw}a(\lambda)N(z, t)$$
$$\Delta\gamma_i = \left(a(\lambda)N(z, t) - b(\lambda)\right)\left(1 - \epsilon(I_F + I_B)\right)$$
$$I_{F,B} = \int\int \frac{1}{2Z_{\mathrm{char}}}\left|R_{F,B}\right|^2 dx\, dy \quad (14)$$

where Z_{char} is the characteristic impedance. All parameters used in the above formula are explained in Table I. Spectral hole burning is included via the $(1 - \epsilon(I_F + I_B))$ factor. I_F and I_B are expressed in watts and they represent the total local forward or backward traveling power, ϵ is then expressed in $[\mathrm{W}^{-1}]$. The choice of the z axis origin is shown in Fig. 6, it is taken at a top of the grating. The length L of the laser is assumed to be a whole number of grating periods $L = l\,\Lambda$. In practice this is not realizable. Therefore the displacement of the real facets with respect to the reference planes introduced at $z = o$ and $z = L$ (both at a top of the grating), is accounted for in the reflection coefficients ρ_f and ρ_b. As indicated in the insets of Fig. 6, $\rho_i = \rho_{io}\exp\left(-j2\pi\Delta_i/\Lambda\right)$ $(i = f, b)$, in which ρ_{io} is the reflectivity at the facet (including coatings) and in which the phase factor expresses the displacement of the facet with respect to the reference plane.

Spontaneous emission has been neglected in the field equations, because its influence is weak and is only important when side-mode suppression is to be examined in an exact way. The terms Δn_r and Δn_i represent the variations in real and imaginary part of the refractive index due to changes in the carrier density. This carrier density $N(z, t)$ is time dependent and can vary with position. The carrier dynamics are given by the following rate equation,

TABLE I

Parameter		Typical Value	
α_{lw}		6	Linewidth enhancement factor
α_{int}	[μm^{-1}]	50×10^{-4}	Internal waveguide losses
B	[$\mu m^3/s$]	100	Bimolecular recombination
C	[$\mu m^6/s$]	20×10^{-5}	Auger recombination
d	[μm]	0.12	Active layer thickness
ϵ	[W^{-1}]	0 or 1	Gain-suppression coefficient
$h\nu$	[eV]		Photon energy related to λ
ϕ_{mf}		$[-\pi, \pi]$	Phase of reflectivity ρ_f
ϕ_{mb}		$[-\pi, \pi]$	Phase of reflectivity ρ_b
Γ		0.5	Power confinement factor in active layer
κ_{FB}	[μm^{-1}]	6.6×10^{-3}	Coupling coefficient backward to forward propagating wave
κ_{BF}	[μm^{-1}]	6.6×10^{-3}	Coupling coefficient forward to backward propagating wave
L	[μm]	± 300	Laser length
λ	[μm]		Wavelength of the lasing mode
Λ	[μm]	0.2422	Grating period
n_c		3.25	Unperturbated effective refractive index
η		0.8	Current injection efficiency
q	[Coulomb]	1.6×10^{-19}	Electron charge
τ	[s]	5.0×10^{-9}	Carrier lifetime
ρ_b			Field reflectivity at left (or back) facet
ρ_f			Field reflectivity at right (or front) facet
R_b		0.32	Power reflectivity at left facet
R_f		0, 0.05, 0.32	Power reflectivity at right facet
v_g	[$\mu m/s$]	7.46×10^{13}	Group velocity
w_y	[μm]	1.5	Stripe width

gain $= a(\lambda)N - b(\lambda)$ [μm^{-1}]

with $a(\lambda) = 0.88\ 10^{-6}\ (h\nu - 0.752)^{0.9513}$ [μm^2]

$b(\lambda) = 163.22\ (h\nu - 0.668)^{3.793}$ [μm^{-1}]

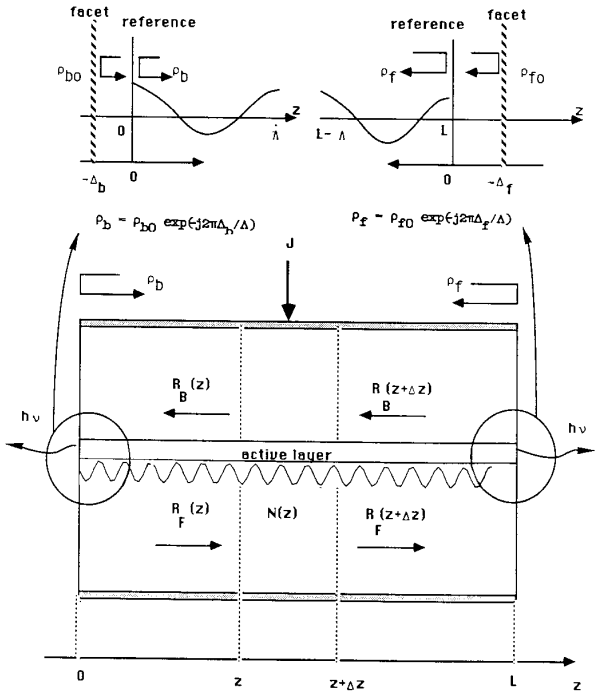

Fig. 6. Longitudinal cross section of a DFB laser.

in which the longitudinal diffusion term has been neglected because the diffusion length is short as compared to the axial variations.

$$\frac{\partial N(z,t)}{\partial t} = \frac{\eta J}{qd} - \frac{N}{\tau} - BN^2 - CN^3 - \frac{\Gamma \Delta\gamma_i(\lambda, z, t)}{h\nu\, dw_y}\left(I_F(z,t) + I_B(z,t)\right). \tag{15}$$

The parameters are again explained in Table I. The injected current density is represented by J, and is assumed to be uniform in the DFB lasers considered here.

Equations (12)–(15) fully determine the static and dynamic behavior of the laser. Fabry–Perot lasers can also be described by this model by simply setting the coupling constants to zero.

As it is our intention to perform a small-signal analysis, we first need to solve the static laser problem in some bias point. Then, we can proceed towards an ac analysis. In the next section we will outline the solution method for the static equations.

B. Above-Threshold Static Analysis of the DFB Laser

The static problem is obtained by omitting the time derivatives in (12)–(15). The computer model we developed is based on the well-known propagator-matrix formalism [17] for the solution of the coupled-wave equations. To take into account spatial variations of the carrier density along the cavity, the device is divided into many small sections of length Δz (see Fig. 6), in which the carrier density is considered to be uniform. For each section a propagator matrix is calculated using the local carrier density. The lasing wavelength and optical power level are found by transforming the boundary value problem (12), (13) into an initial value problem that is solved with an iterative shooting method.

The calculation proceeds as follows. First, initial estimates are introduced for the lasing wavelength λ and the field $R_B(0)$, which can be taken real without any restriction. Applying the left boundary condition gives a starting value for the field $R_F(0)$. Both backward and forward waves are now propagated through the laser taking the photon–carrier interaction into account self-consistently. At the right facet the second boundary conditions requires $R_B(L) - \rho_f R_F(L)$ to be zero. Since the propagation implies that $R_B(L)$ and $R_F(L)$ are both complex functions of the real variables λ and $R_B(0)$, it is clear that we have to find the appropriate zero of a function f, defined as

$$f(\lambda, R_B(0)) = R_B(L)(\lambda, R_B(0)) - \rho_f R_F(L)(\lambda, R_B(0)). \tag{16}$$

A Newton–Raphson (NR) technique is applied to find this zero starting from the initial estimates. The derivatives needed in this NR-algorithm are calculated by an additional propagation of the $\partial R_{F,B}(z)/\partial\lambda$ and

$\partial R_{F,B}(z)/\partial R_B(0)$ derivatives. The above principle can be used for a multimode approach.

C. Small-Signal Analysis of the DFB Laser

The usual approach towards the small-signal analysis is the sinus regime, written in the phasor notation. However, before complex phasors related to the modulation frequency $\Omega/2\pi$ can be introduced, the complex notation with respect to the lasing frequency ω must be removed. Therefore R_F and R_B are replaced by

$$R_{F,B}(z, t) = r_{F,B}(z, t)e^{j\phi_{F,B}(z,t)+j\int_t \Delta\omega(t')dt'} \quad (17)$$

in which the functions r_F, r_B, ϕ_F, ϕ_B, and $\Delta\omega$ are all real; $\Delta\omega(t)$ represents the wavelength chirp (further on this will correspond to the FM response). Because of the explicit presence of the chirp in the phase of $R_{F,B}$, the term $\phi_{F,B}$ is fixed to not include chirp by boundary conditions which are imposed later [in (20)]. The traveling-wave equations for r_F and ϕ_F become (with $\Delta\beta = \Delta\beta_r + j\Delta\beta_i$)

$$\frac{\partial r_F}{\partial z} + \frac{1}{v_g}\frac{\partial r_F}{\partial t} - \Delta\beta_i r_F = |\kappa_{FB}| \sin(\phi_{FB} + \phi_B - \phi_F) r_B \quad (18)$$

$$\frac{\partial \phi_F}{\partial z} + \frac{1}{v_g}\frac{\partial \phi_F}{\partial t} + \frac{1}{v_g}\Delta\omega + \Delta\beta_r = -\frac{r_B}{r_F}|\kappa_{FB}| \cos(\phi_{FB} + \phi_B - \phi_F). \quad (19)$$

ϕ_{FB} is the phase of κ_{FB}. For r_B and ϕ_B similar equations hold. The boundary conditions (13) are transformed into

$$r_F(0, t) = |\rho_b| r_B(0, t), \qquad r_B(L, t) = |\rho_f| r_F(L, t)$$
$$\phi_F(0, t) = \phi_{mb}, \ \phi_B(0, t) = 0$$
$$\phi_B(L, t) = \phi_F(L, t) + \phi_{mf} + 2\pi m - 2\beta_g L$$
$$m = 0, \pm 1, \pm 2, \cdots. \quad (20)$$

The sinus regime is now introduced by linearizing (15), (18), (19), and (20) around some bias point, using

$$r_{F,B}(z, t) = r_{F,B,o}(z) + \mathrm{Re}\left(\Delta r_{F,B}(z, \Omega) e^{j\Omega t}\right)$$
$$\phi_{F,B}(z, t) = \phi_{F,B,o}(z) + \mathrm{Re}\left(\Delta\phi_{F,B}(z, \Omega) e^{j\Omega t}\right)$$
$$N(z, t) = N_o(z) + \mathrm{Re}\left(\Delta N(z, \Omega) e^{j\Omega t}\right)$$
$$J(t) = J_o + \mathrm{Re}\left(\Delta J e^{j\Omega t}\right)$$
$$\Delta\omega(t) = \mathrm{Re}\left(\Delta\omega(\Omega) e^{j\Omega t}\right). \quad (21)$$

The terms with the subscript (o) belong to the static solution, while the other terms are small-signal complex phasors for the ac analysis; $\Omega = 2\pi f$ with f the modulation frequency. We will not give the linearized equations because they are too extended although their derivation is straightforward. The equations thus obtained form a linear set that can be solved with standard techniques. $\Delta\omega(\Omega)$ describes the FM response of the laser, while the IM response can be deduced from $\Delta r_B(0, \Omega)$ and $\Delta r_F(L, \Omega)$.

V. Modeling Examples

The FM response of both the FP laser and DFB laser will be examined. The most important parameters used in the model are specified in Table I. Other values than these will be specified explicitly in the text. Spontaneous emission is omitted in the analysis.

A. The Fabry-Perot Laser

Although the FP laser has already been investigated thoroughly, we include this topic for two reasons, first as a verification of our model and secondly to demonstrate the general phenomena of longitudinal carrier density modulations. Two cases are considered, one with ($\epsilon = 1$ W^{-1}) and one without ($\epsilon = 0$ W^{-1}) spectral hole burning, i.e., gain suppression. In Fig. 7(a) and (b) the amplitude and phase of the FM response (i.e., the amplitude and phase of $\Delta\omega/\Delta I$) versus modulation frequency are drawn for several bias currents. The results agree with literature [18]: without spectral hole burning $\Delta\omega$ goes to zero as Ω decreases, in the other case a flat response occurs at low modulation rates and the resonances are damped more strongly.

As expected (see Section III), spatial hole burning shows no effect on the FM response. It is however interesting to take a closer look at the internal behavior of the carriers. To remove the influence of spectral hole burning we depict the small-signal carrier density $\Delta N(z, \Omega)$ for the $\epsilon = 0$ W^{-1} case. Fig. 8(a) shows the amplitude of $\Delta N(z, \Omega)$ as a function of z and Ω and Fig. 8(b) shows its phase. In contrast to the FM response (Fig. 7, case with $\epsilon = 0$ W^{-1}) the local small-signal carrier density modulation does not approach zero as Ω drops and moreover it fluctuates along the z axis [Fig. 8(a) and (b)]. In a classical rate equation model [8] the (average) small-signal carrier density would be zero. This means that at low modulation frequencies the in-phase with injected current and out-of-phase areas, respectively, phase zero and phase π for low Ω in Fig. 8(b), must compensate each other.

As indicated by the arrow in Fig. 8(a), at higher frequencies there is a cutoff of the spatial hole burning in the small-signal carrier distribution. This is confirmed by the uniform behavior of the carrier density ΔN for higher frequencies.

None of these internal spatial hole burning effects are observed in the FM response.

B. The DFB Laser

In this section a number of case studies on different DFB devices is described, in particular, with the aim of elucidating the effect of longitudinal spatial hole burning on the FM response.

Examples of Calculated Devices: The FM response of approximately a dozen different DFB devices was studied. Besides, for some devices, we checked the sensitivity of their behavior to variations in chosen parameter values. In total about 50 devices were calculated.

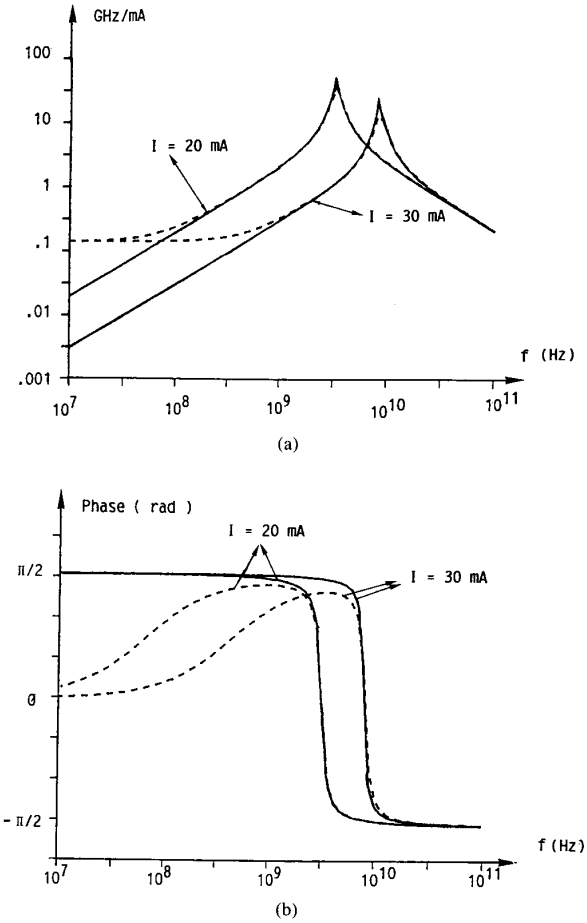

Fig. 7. (a) Amplitude and (b) phase of the FM response of a Fabry–Perot laser for two bias currents. The solid line indicates without spectral hole burning while the broken line indicates with spectral hole burning.

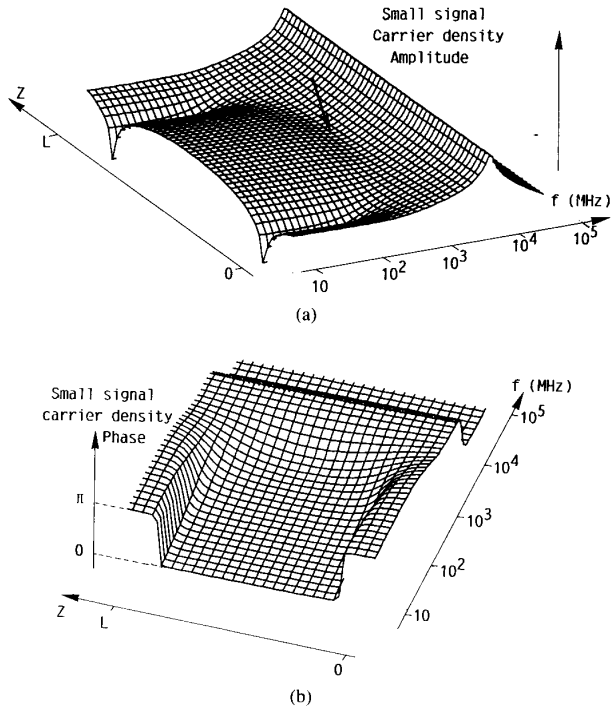

Fig. 8. Small-signal carrier density distribution (a) amplitude and (b) phase in the longitudinal direction versus modulation frequency for a Fabry–Perot laser and for I_{bias} = 20 mA (I_{th} = 18.2 mA).

TABLE II
DFB LASER EXAMPLES

Case	R_b	ϕ_b	R_f	ϕ_f	ϵ [W^{-1}]	I_{th} [mA]	λ_{th} [μm]	$\Delta\alpha L$
A_o	0.32	$-\pi/4$	0	—	0	24.14	1.56045	0.32
A_1	0.32	$-\pi/4$	0	—	1	24.14	1.56045	0.32
B_o	0.32	$\pi/2$	0.05	0	0	21.24	1.56110	0.28
B_1	0.32	$\pi/2$	0.05	0	1	21.24	1.56110	0.28

Detailed results for two devices are presented here. Both devices have a κL of 2 and a 32 percent back-facet reflectivity. One device (labeled A) has an ideal AR coating on the front facet, whereas the other (labeled B) has a 5 percent front-facet reflectivity. The choice we made for the facet phases for both devices is random, except that we checked the devices for a large threshold gain difference between main mode and side mode. The difference $2\Delta\alpha L$ is 0.64 for A and 0.56 for B. According to [12] this guarantees genuine single-mode operation over a wide power range.

For both devices the FM response is calculated with spatial hole burning always present. In order to emphasize the effect of spatial hole burning, calculations with and without simultaneous spectral hole burning were done. The devices A and B without spectral hole burning are denoted A_o and B_o in the text, with spectral hole burning they are denoted A_1 and B_1, respectively. (An index 1 is chosen deliberately; it corresponds to a spectral hole burning gain suppression coefficient ϵ of about 1 W^{-1}.) Common parameter values of devices A and B are given in Table I, whereas the parameters, which have different values for the two devices, are listed in Table II.

The Carrier Density Modulations: Obviously, the nonuniform longitudinal distribution of the modulated carrier density forms the basis for the spatial hole burning contribution to the FM response. As an example, the small-signal carrier density modulations $\Delta N(z, \Omega)$ for devices A and B at a bias of 30 mA are depicted in Figs. 9 and 10. Spectral hole burning turns out to have negligible influence on the spatial distributions of $\Delta N(z, \Omega)$; the index 0 or 1 is therefore immaterial in these plots. At first glance we somewhat surprisingly find the spatial hole burning component of these carrier density modulations to be very similar for all devices and there is not much difference from the longitudinal carrier density modulation along the FP laser, as shown in Fig. 8(a) and (b). The main difference with the FP is in the spatial distribution of the phase at low frequency. Along the cavity of the FP the phase subsequently is π, 0, π. For the DFB's A and B it is the

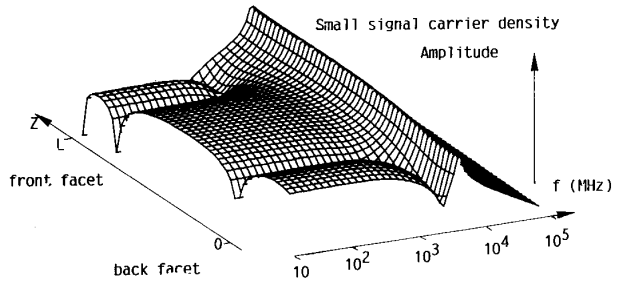

Fig. 9. Small-signal carrier density distribution (amplitude) in the longitudinal direction versus modulation frequency for device A_o (R_f = 0 percent, R_b = 32 percent, no spectral hole burning) for I_{bias} = 30 mA.

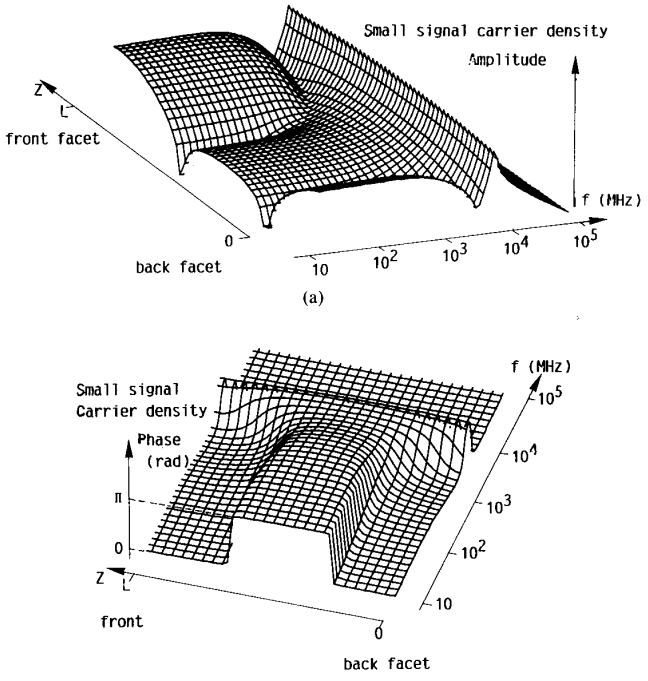

Fig. 10. Small-signal carrier density distribution in the longitudinal direction versus modulation frequency for device B_o (R_f = 5 percent, R_b = 32 percent, no spectral hole burning) for I_{bias} = 30 mA. (a) Amplitude, (b) phase.

other way around: 0, π, 0 (see Fig. 10(b) for device B). We would also speculate that DFB's with a π, 0, π distribution can be found, presumably, e.g., for DFB's with two uncoated facets (or at lower κL or at other facet phases). Further note that for the DFB's A and B as well as for the FP laser, the amplitude of the carrier density modulation at intermediate frequency (well below the relaxation oscillation) only shows a dip at positions where the low-frequency phase is zero (i.e., carrier density modulation in-phase with the current modulation).

For devices B_o and B_1 the static carrier density for a whole range of bias levels is shown in Fig. 11. The local difference between the static carrier density distributions at two subsequent bias levels (at least if they are closely spaced) is the small-signal carrier density in the limit of zero modulation frequency.

The Carrier-Induced FM Response: Despite the large similarity in the spatial hole burning component of the carrier density modulations, the calculations showed that the spatial hole burning contribution to the FM response is totally different for the three devices (the FP and the two DFB's A and B). Obviously it is not the carrier density modulation by itself which matters, but rather it is the overall effect of the carrier density modulation on the round-trip gain and phase conditions of the cavity which counts. This was already demonstrated for the FP laser, where the effect of the spatial hole burning component was shown to be zero. As discussed qualitatively in Sec-

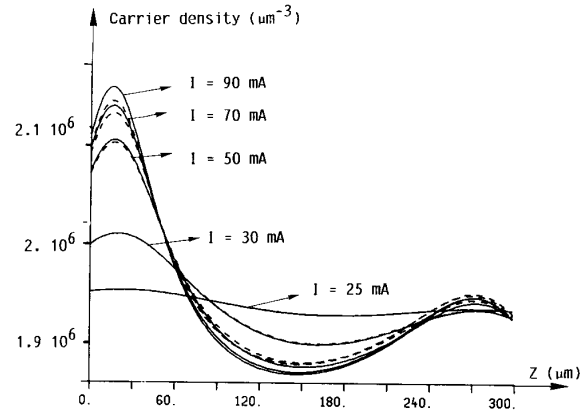

Fig. 11. Static carrier density distribution along z for devices B_o and B_1 for several dc currents. The solid line indicates without spectral hole burning while the broken line indicates with spectral hole burning.

tion III, the effect for DFB's may vary (strongly) from one device to another, depending on facet phase, facet reflectivity, κL, the static carrier density distribution, and possibly also on details of the carrier density modulation. So this explains why the two DFB devices A and B behave very differently in their FM responses.

Spatial Hole Burning Effects: Leaving out the spectral hole burning for a moment, the FM responses for devices A_o and B_o as a function of frequency at various bias levels are shown in Figs. 12 and 13. Devices A_o and B_o do indeed have in common a flat FM response at low frequencies due to spatial hole burning. The level of this response decreases with increasing bias.

As shown in Figs. 12 and 13, the striking difference between A_o and B_o is the phase of the FM at low and intermediate frequencies. At low frequency the FM phase of A_o is π, whereas for B_o it is 0. Associated with this difference in phase, there also is a pronounced difference in the amplitude of the FM versus frequency. Device A_o shows a gradual increase around the GHz; and then a further increase into the relaxation oscillation. However, for device B_o a pronounced dip appears in the FM versus frequency around the GHz, before the relaxation oscillation takes over. Obviously the dip is caused by a rolloff of the spatial hole burning at high frequency. Simultaneously with this dynamic rolloff of the spatial hole burning contribution to $\Delta\omega$, the phase of that FM component will quite abruptly change either from π to $\pi/2$ (case A) or from 0 to $-\pi/2$ (case B). It is then the compound effect of the ever-present term, which increases with Ω and has phase $\pi/2$ below f_r, and the spatial hole burning component, that determines whether or not a dip in the FM versus frequency will occur. When at rolloff both components have phase $\pi/2$, a gradual increase will occur (case A). However when the phase of the terms becomes $\pi/2$ ("ever-present" component), respectively, $-\pi/2$, then a dip will appear (case B).

Simultaneous Spectral and Spatial Hole Burning Effects: Simultaneous inclusion of spectral hole burning

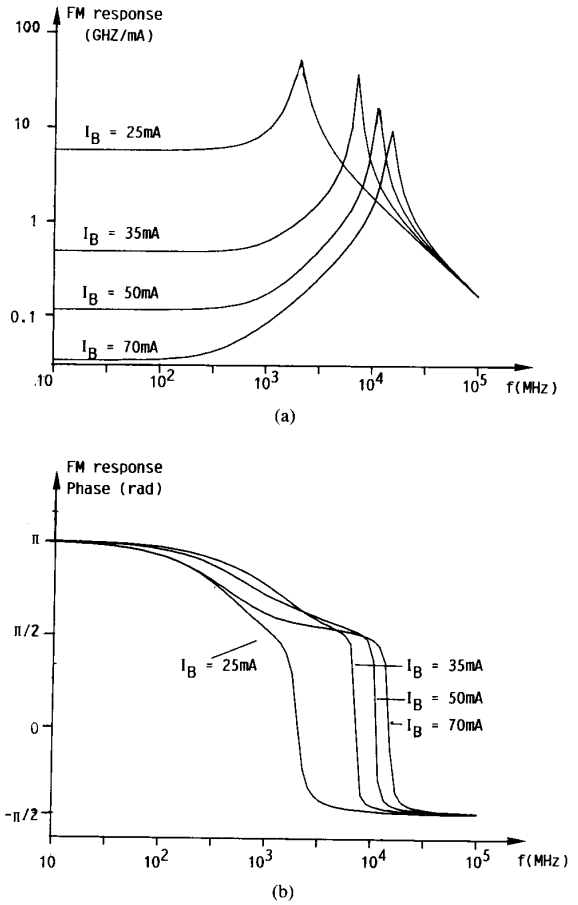

Fig. 12. Amplitude (a) and phase (b) of the FM response of device A_o (R_f = 0 percent, R_b = 32 percent, no spectral hole burning) for several bias currents.

further complicates the FM response, in particular for DFB device A (now A_1). The consequences for B (now B_1) are less pronounced. The calculated FM responses of A_1 and B_1 as a function of frequency at various bias levels are given in Fig. 14 and Fig. 15 (with an ϵ of 1 W^{-1}).

A common feature of the FM response of A_1 and B_1 is that at low to intermediate frequency, the FM response, with increasing bias, now levels off to a constant value (i.e., the spectral hole burning contribution). Upon comparing A_o, B_o (Figs. 12, 13) with A_1, B_1 (Figs. 14, 15), respectively, another common feature is found. At low bias (a few mA above threshold), the simultaneous inclusion of spectral hole burning has little influence and the spatial hole burning dominates the (low and intermediate frequency) FM response.

"Spatially" dominating at low bias, combined with "spectral" dominating at high bias has, for device B_1 produces few further consequences. It only weakens the spatial hole burning dip around the GHz in the FM versus frequency. However, for device A_1 the two contributions apparently cancel almost exactly, at one specific bias level (50 mA). As seen from Fig. 14 at this bias level, the (low

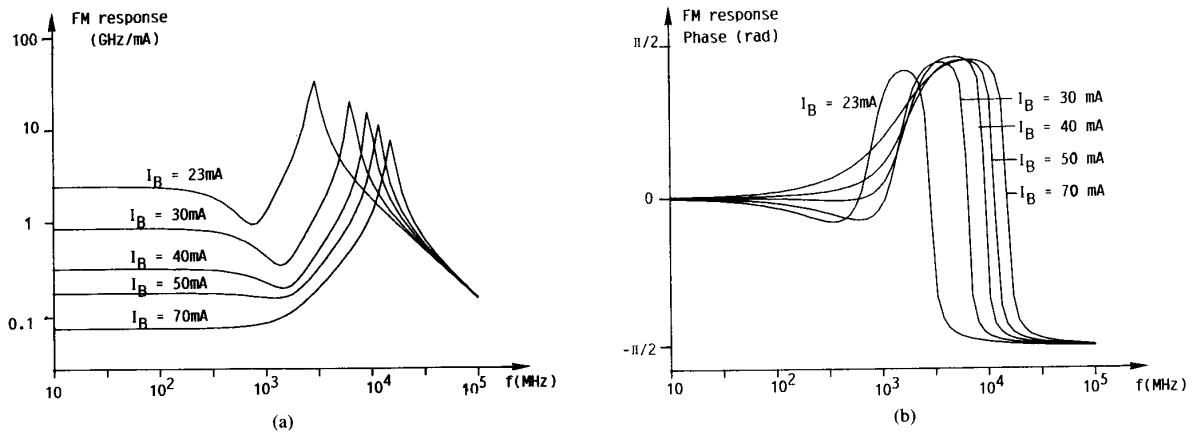

Fig. 13. Amplitude (a) and phase (b) of the FM response of device B_o (R_f = 5 percent, R_b = 32 percent, no spectral hole burning) for several bias currents.

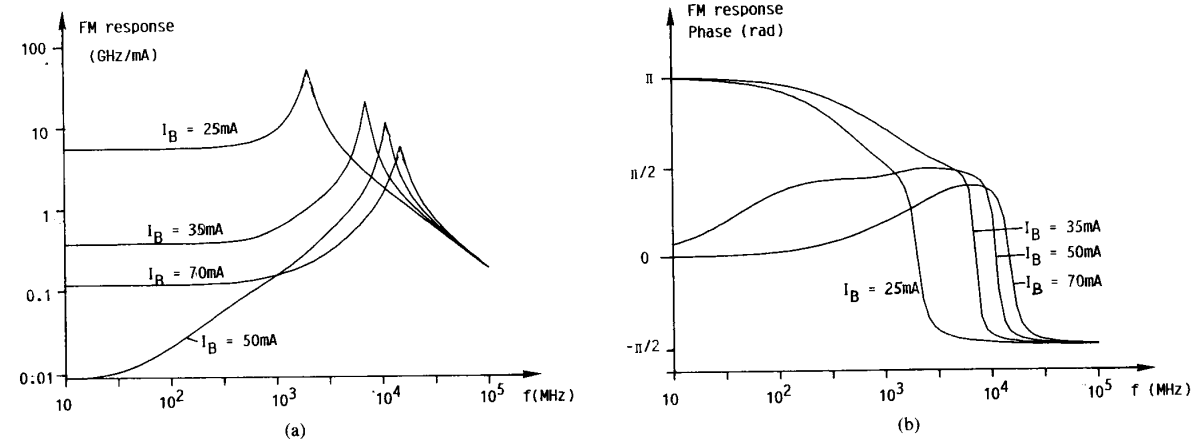

Fig. 14. Amplitude (a) and phase (b) of the FM response of device A_1 (R_f = 0 percent, R_b = 32 percent, with spectral hole burning) for several bias currents.

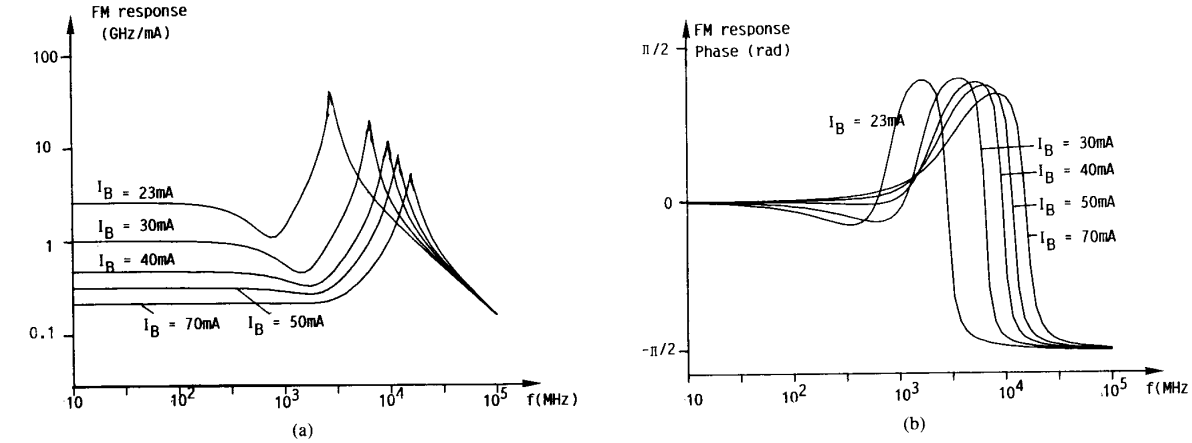

Fig. 15. Amplitude (a) and phase (b) of the FM response of device B_1 (R_f = 5 percent, R_b = 32 percent, with spectral hole burning) for several bias currents.

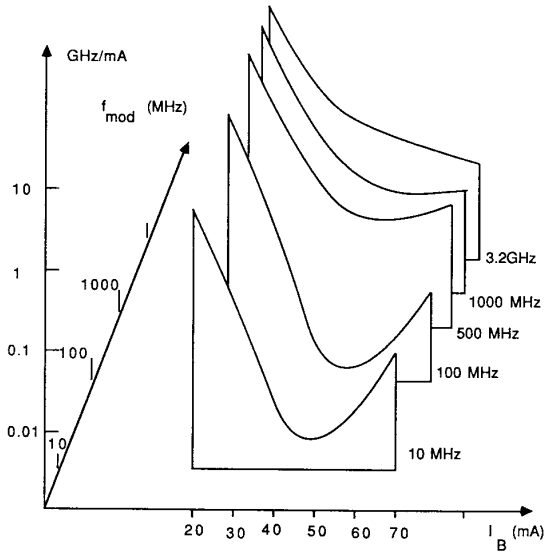

Fig. 16. Perspective view of the FM response versus bias and frequency, for device A_1.

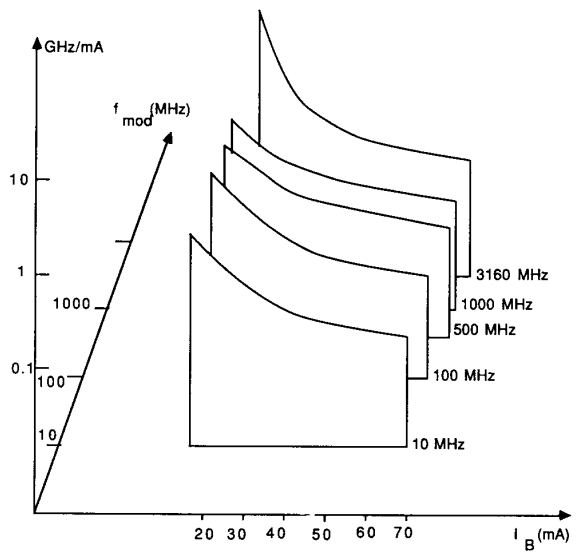

Fig. 17. Perspective view of the FM response versus bias and frequency, for device B_1.

and intermediate) FM is proportional to the frequency and the FM phase is close to $\pi/2$. The large difference in FM as a function of bias between A_1 and B_1 is easy to understand. As can be seen in Fig. 7(b) for the FP laser, the phase of the low-frequency spectral hole burning FM is equal to zero. Hence device B_1 has the phases: "spectral" 0/"spatial" 0, whereas device A_1 has: "spectral" 0/"spatial" π. Therefore, only for device A_1 a spatial hole burning FM, decreasing with bias, can be compensated for by a constant spectral hole burning FM, at one specific bias level. At this bias level then only the "everpresent" contribution to the FM is retained (see also Section III) and a pronounced dip will occur in the FM versus bias.

A perspective view of the calculated FM responses of devices A_1 and B_1 as a function of frequency and bias is given in Figs. 16 and 17, respectively. Such in order to facilitate comparison of the gross features with experimentally determined FM responses of DFB lasers (e.g., Fig. 1(a)–(c)).

The Thermally-Induced FM: Although thermal contributions to the FM response at lower frequencies (below say 10 MHz) are outside the scope of this paper, we want to point out the way they may interfere with spectral and spatial hole burning FM. In the FM, the thermal contribution and the spectral one are out-of-phase. Since the magnitude of the low-frequency thermal contribution is always larger than the spectral one, this would lead to a dip in the FM response somewhere around the MHz. However this dip will disappear if there is a spatial hole burning contribution, dominating over the spectral contribution in the 100 MHz–1 GHz range and which by chance is also out-of-phase with the spectral, and hence in-phase with the thermal.

Obviously, for a very large spatial contribution to the FM (which also dominates over the low-frequency thermal FM) the spectral/thermal dip around the MHz will always disappear, irrespective of the "spatial" phase.

VI. Comparison of Theory and Experiment

Generally, there is a good qualitative agreement between the experimental and theoretical results on the carrier-induced FM response of DFB lasers. The 12 modeling examples confirm that the dynamic FM behavior can strongly vary from chip to chip.

A striking resemblance between theory and experiment is the occasional occurrence of the dip in the FM versus bias, where "spectral" and "spatial" cancel each other. The experimental device of Fig. 1(b), as well as the theoretical device A_1 of Fig. 16 show this feature.

Another strong similarity between theory and experiment is the occasional occurrence of a rolloff (slightly above the GHz) in the FM versus frequency at elevated bias. This rolloff occurs in conjunction with a high FM level at low bias, while in the FM versus bias no dip (due to "spectral"/"spatial" cancellation) appears. Both the experimental device of Fig. 4 and the theoretical device B_1 (or B_0) of Fig. 15 (Fig. 13) show the rolloff. The time scale of the rolloff is about the same (0.1 ns) where the measured and with the model calculated lifetime at threshold are, respectively, 0.7 and 0.9 ns

By no means, do all experimental or theoretical devices show such a dominating spatial hole burning contribution, be it either out- or in-phase with the "spectral" FM. For instance the experimental device of Fig. 1(a) [Fig. 2(a)] only has a relatively weak "spatial" FM contribution, in-phase with the "spectral" FM at low frequency. This leads to a slight rolloff around the GHz in the FM versus frequency and also a slight decrease with bias (at low frequency around 200 MHz). But the gross features still are

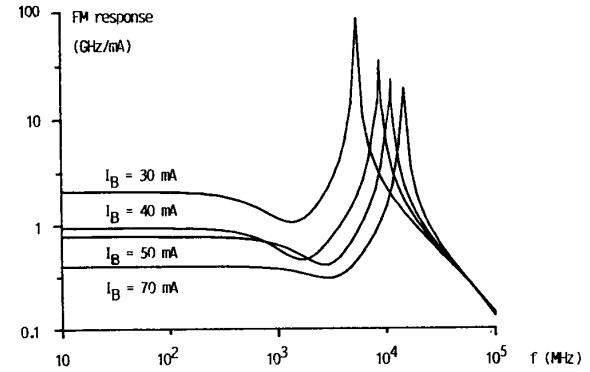

Fig. 18. Amplitude of the FM-response of a $\lambda/4$-shifted DFB laser (with $R_f = R_b = 0$ percent and $\epsilon = 1\ W^{-1}$) for several bias currents.

rather characteristic for a dominating spectral hole burning contribution to the FM. Theory however does not exclude this possibility.

At some points there are discrepancies between theoretical and experimental data. For virtually all biases the theoretical results show a really flat FM response from 100 up to about 600 MHz. Experimentally in many cases it is only approximately flat, with variations of the order of a dB. Furthermore, in theory the strength of the spatial hole burning contribution to the FM response always appears to decrease with increasing bias. For some experimental devices one would rather conclude an increase of the strength of the "spatial" with bias.

The calculated examples shown have one AR-coated and one uncoated facet and a κL of 2. The power reflection coefficient of the coated facets varied between 0 and 5 percent. For all of these examples the level of the spatially-induced FM component is quite similar. Presumably this relates to the κL-product being the same for the calculated examples. For most (not all) values of ϕ_b and/or ϕ_f (at least those for which a stable-single-mode static behavior occurs) the 0 percent AR-coating gives phase π for the low-frequency spatial FM, while the 5 percent AR-coating gives phase 0. This suggests a stronger dependence on the level of the reflectivity than on its phase. Further calculations are needed however, to investigate this issue in detail and to see how the level and the phase of the spatial FM are affected by the amplitude and the phase of the end reflections for higher reflectivities of the coated facet.

From a fabrication yield and mode selectivity point of view the $\lambda/4$-shifted DFB laser with good AR coatings looks like a favored device. Moreover these devices should have deterministic FM-responses. A preliminary calculation of the FM-response of a $\lambda/4$ shifted laser is shown in Fig. 18. The laser has two perfect AR-coatings and $\epsilon = 1\ W^{-1}$. All other parameters are mentioned in Table I. Again observe the bias dependent spatial hole burning contribution to the FM which has a zero low-frequency phase (not shown) so that no dip occurs in the FM versus bias characteristic. In devices with a dominant "spectral" FM the bias dependent spatial FM will be screened by the "spectral" FM causing a smaller overall bias dependence.

Finally it ought to be mentioned that many minor effects that are not included in the model, might contribute to the FM while hardly affecting the IM. We mention: a wavelength and carrier dependent linewidth enhancement factor, small local heating effects, nonuniform current injection, effects due to side modes on a 30 dB down level, coupling between longitudinal and lateral spatial hole burning, and technological imperfections.

VII. Conclusion

We have made a comprehensive analysis of the carrier-induced FM response of DFB lasers.

Experimentally we have shown that the FM response may sometimes vary strongly from chip to chip. In a number of instances anomalies either as a function of frequency or as a function of bias were observed.

Theoretically a new dynamic model was presented which includes spectral as well as longitudinal spatial hole burning. Its main feature is that local variations of the Bragg wavelength, due to variations in the carrier density, are rigorously and self-consistently taken into account.

Various calculations with this model confirmed that spatial hole burning can deliver an important contribution to the carrier-induced FM response in DFB lasers. In contrast with the spectral hole burning and "ever-present" (relaxation oscillation) contribution, spatial hole burning can cause either a red or blue frequency shift. Which of the two possibilities occurs, depends on the facet reflectivity (modulus and phase), κL and so on, as does the actual strength of the "spatial" contribution to the FM.

By comparing our experimental results with the theoretical calculations, the anomalies that are found experimentally in the FM versus frequency and FM versus bias were explained as the combined effect of the different contributions to the carrier-induced FM response. The dip or rolloff in the low GHz range of the FM versus frequency is caused by the dynamic rolloff of the spatial hole burning component and the relative phases between the FM contributions. More particularly the rolloff will appear when a sufficiently strong "spatial" contribution occurs in-phase with the "spectral" component (phase 0) at low frequency and is due to the interference of the "ever-present" and spatial hole burning FM components. The FM versus bias then just shows a slight decrease in the FM efficiency with bias. The dip in FM versus bias is due to the bias dependence of the amplitude of the spatial hole burning contribution and the possible phase difference between spatial and spectral hole burning components. Hence, when "spatial" and "spectral" contributions are out-of-phase a strong dip may occur in the FM versus bias characteristic. Then, at one specific bias level "spatial" and "spectral" contributions cancel each other and only the "ever-present" contribution is retained.

Because the mirror phase is an unknown, it is hard to predict the FM response of individual DFB lasers. Statis-

tical considerations then are useful and/or necessary. On the other hand the $\lambda/4$ shifted DFB lasers with good AR coatings seem promising for deterministic FM responses.

APPENDIX

An estimate of the rolloff frequency and of the bias dependence of the spatial hole burning follows from the rate equation of the carriers:

$$\frac{dN}{dt} = J - \frac{N}{\tau} - GP. \tag{22}$$

To reduce complexity we will neglect here the spectral hole burning and set the gain equal to

$$G = \frac{\partial G}{\partial N}(N - N_{\text{tr}}),$$

$$N_{\text{tr}} = \text{transparency carrier density}. \tag{23}$$

Further the field intensity is assumed to have a spatial distribution of the form

$$P(z, t) = P_a(t)\big(1 + f(z)\big) \tag{24}$$

where f is some function for which $\int f\,dz = 0$ holds. The spatial hole burning can now be approximated by expanding the spatial carrier distribution to the first order in f:

$$N(z, t) = N_a(t) + N_1(t) f(z). \tag{25}$$

Inserting (23)–(25) in (22) gives, after some manipulations the rate equation for N_1:

$$\frac{dN_1}{dt} = -\frac{N_1}{\tau} - \zeta \frac{\partial G}{\partial N} P_a N_1 - \frac{\partial G}{\partial N}(N_a - N_{\text{tr}}) P_a \tag{26}$$

with

$$\zeta = 1 - \frac{1}{l^2}\int \frac{dz}{f}\int f^2\,dz, \qquad l = \text{laser length}. \tag{27}$$

We introduce now the small-signal phasor representation by writing $P_a = P_{a,o} + p e^{j\Omega t}$, $N_a = N_{a,o} + n_a e^{j\Omega t}$, and $N_1 = N_{1,o} + n_1 e^{j\Omega t}$. Equation (26) can then be written as

$$\left(j\Omega + \frac{1}{\tau} + \zeta \frac{\partial G}{\partial N} P_{a,o}\right) n_1 = -\frac{\partial G}{\partial N}\left((N_{a,o} + \zeta N_{1,o} - N_{\text{tr}})p + P_{a,o} n_a\right). \tag{28}$$

As seen from the left-hand side of this expression, the spatial hole burning, here represented by n_1, shows a 3 dB rolloff at a frequency of $[1/\tau + \zeta(\partial G/\partial N) P_{a,o}]$. With increasing bias ($P_{a,o}$) there is apparently a decrease of the low-frequency spatial hole burning and simultaneously an increase of the rolloff frequency.

ACKNOWLEDGMENT

The authors wish to thank W. Dijksterhuis, T. van Dongen, H. P. M. Ambrosius, G. L. A. van der Hofstad, and J. J. M. Binsma for their contributions and the fabrication of the DFB devices and J. P. Van de Capelle for his support in developing the dc model.

REFERENCES

[1] J. E. Bowers, W. T. Tsang, T. L. Koch, N. A. Olsson, and R. A. Logan, "Microwave intensity and frequency modulation of heteroepitaxial-ridge-overgrown distributed feedback lasers," *Appl. Phys. Lett.*, vol. 46, pp. 233–235, Feb. 1985.

[2] R. S. Vodhanel, N. K. Cheung, and T. L. Koch, "Direct frequency modulation of vapor phase transported distributed feedback semiconductor lasers," *Appl. Phys. Lett.*, vol. 48, pp. 966–968, Apr. 14, 1986.

[3] S. Murata, I. Mito, and K. Kobayashi, "Frequency modulation and spectral characteristics for a 1.5 μm phase-tunable DFB laser," *Electron. Lett.*, vol. 23, pp. 12–14, Jan. 2, 1987.

[4] Y. Yoshikuni and G. Motosugi, "Multielectrode distributed feedback laser for pure frequency modulation and chirping suppressed amplitude modulation," *J. Lightwave Technol.*, vol. LT-5, pp. 516–522, Apr. 1987.

[5] H. Nishimoto, M. Yamaguchi, I. Mito, and K. Kobayashi, "High-frequency response for DFB LD due to wavelength detuning effect," *J. Lightwave Technol.*, vol. LT-5, Oct. 1987.

[6] E. Goobar, L. Gillner, R. Schatz, B. Broberg, S. Nilsson, and T. Tanbun-Ek, "Measurement of a VPE-transported DFB laser with blue-shifted frequency modulation response from DC to 2 GHz," *Electron. Lett.*, vol. 24, pp. 746–747, June 9, 1988.

[7] X. Pan, H. Olesen, and B. Tromborg, "FM characteristics of multielectrode DFB and DBR lasers," presented at the 11th IEEE Semiconductor Laser Conf., Aug. 1988.

[8] R. S. Tucker, "High-speed modulation of semiconductor lasers," *IEEE Trans. Electron Devices*, vol. ED-32, pp. 2572–2584, Dec. 1985.

[9] A. Valster, L. J. Meuleman, P. I. Kuindersma, and T. V. Dongen, "Improved high frequency response of InGaAsP DCPBH lasers," *Electron. Lett.*, vol. 22, pp. 16–18, 1986.

[10] C. H. Henry, "Theory of the phase noise and power spectrum of a single mode injection laser," *IEEE J. Quantum Electron.*, vol. QE-19, pp. 1391–1397, Sept. 1983.

[11] —, "Theory of linewidth of semiconductor lasers," *IEEE J. Quantum Electron.*, vol. QE-18, pp. 259–264, 1982.

[12] A full statistical analysis for DFB's can, e.g., be found in: P. I. Kuindersma, P. P. G. Mols, W. V. Es, and I. A. F. Baele, "50 000 different DFB devices," *Proc. ECOC*, 1988, Brighton, England, pp. 384–387. A more extensive account is to be found in P. P. G. Mols, P. I. Kuindersma, W. v. Es-Spiekman, and I. A. F. Baele, "Yield and device characteristics of DFB lasers: Statistics and novel coating design in theory and experiment," *IEEE J. Quantum Electron.*, vol. 25, pp. 1303–1313, June 1989, and references therein.

[13] A. Hermann Haus and C. V. Shank, "Antisymmetric taper of distributed feedback lasers," *IEEE J. Quantum Electron.*, vol. QE-12, pp. 532–539, Sept. 1976.

[14] H. Soda, Y. Kotaki, H. Sudo, H. Ishikawa, S. Yamakoshi, and H. Imai, "Stability in single longitudinal mode operation in GaInAsP/InP phase-adjusted DFB lasers," *IEEE J. Quantum Electron.*, vol. QE-23, pp. 804–814, June 1987.

[15] M. Schubert and B. Wilhelmi, *Nonlinear Optics and Quantum Electronics*. New York: Wiley, 1986, ch. 1, sect. 1.4.2.

[16] A. Yariv, "Coupled-mode theory for guided-wave optics," *IEEE J. Quantum Electron.*, vol. QE-9, pp. 919–933, Sept. 1973.

[17] M. Yamada and K. Sakuda, "Analysis of almost-periodic distributed feedback slab waveguides via a fundamental matrix approach," *Appl. Opt.*, vol. 26, pp. 3474–3478, Aug. 15, 1987.

[18] K. Kishino, S. Aoki, and Y. Suematsu, "Wavelength variation of 1.6 μm wavelength buried heterostructure GaInAsP/InP lasers due to direct modulation," *IEEE J. Quantum Electron.*, vol. QE-18, pp. 343–350, Mar. 1982.

Patrick Vankwikelberge was born in Ghent, Belgium, on May 20, 1962. He received the degree in electrical engineering from the University of Ghent in 1985.

He is presently working toward the Ph.D. degree in electrical engineering at the Laboratory for Electromagnetism and Acoustics, University of Ghent, where he is engaged in the research on the dynamic behavior of semiconductor lasers.

Filip Buytaert, photograph and biography not available at the time of publication.

Ann Franchois, photograph and biography not available at the time of publication.

Roel Baets (M'89) received the degree in electrical engineering from the University of Ghent, Belgium, in 1980, the M.Sc. degree in electrical engineering from Stanford University, Stanford, CA, in 1981, and the Ph.D. degree from the University of Ghent in 1984.

Since 1984 he has been with the Interuniversity Micro-Electronics Centre (IMEC) and works in the Laboratory of Electromagnetism and Acoustics at the University of Ghent, where he is head of research on optoelectronic devices. He lectures part-time courses on optoelectronics at the University of Ghent. His interests include both the theory and technology of optoelectronic devices, especially laser diodes and optical waveguides and switches.

Dr. Baets is a member of the Optical Society of America.

P. I. Kuindersma, for a photograph and biography, see p. 1312 of the June 1989 issue of this JOURNAL.

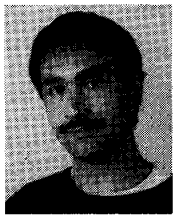

C. W. Fredriksz received the Ing. degree in applied physics from HTS Rijswijk, The Netherlands, in 1984.

He has been with Philips Research Laboratories, Eindhoven from 1984 to the present. From 1984 to 1987 he worked on long wavelength semiconductor lasers for optical communication. Since 1987 he has been involved in the characterization of materials and devices grown by silicon molecular beam epitaxy.